Optical Study of Ultrasonic Diffraction and Focusing in Anisotropic Media

M. G. COHEN
Bell Telephone Laboratories, Incorporated, Murray Hill, New Jersey
(Received 26 April 1967)

This paper describes an investigation of the diffraction of 100–500-Mc/sec longitudinal elastic waves in anisotropic materials, using the techniques of optical (Bragg) scattering, which allow direct measurement of ultrasonic intensity distributions along the path of the beam. Such measured distributions for beams propagating along pure mode axes in crystal quartz, silicon, and potassium bromide are shown to agree very well with intensity distributions predicted using a diffraction integral derived from a rigorous solution of the related problem of electromagnetic diffraction in uniaxially anisotropic media. In addition, it is demonstrated that cylindrical crystal surfaces, symmetric about the proper pure-mode axis, are appropriate excitation surfaces for cylindrically focused ultrasonic beams. The focusing properties of thin-film CdS and ZnO transducers evaporated on cylindrical surfaces of crystal quartz and silicon are described and compared with the properties of focused beams in isotropic materials.

INTRODUCTION

Extensive studies of the propagation of plane elastic waves in anisotropic media[1] have contributed to the successful application of pulsed ultrasonic reflection techniques to measurements in single crystals.[2] Waterman's analysis[3] in particular allows straightforward determination of the particle displacement, velocity, and energy flow direction for plane waves propagating in directions close to a pure-mode axis. In a recent series of papers, Papadakis[4] has studied ultrasonic diffraction in anisotropic materials by introducing Waterman's results into the Rayleigh diffraction integral for isotropic media. Then, using a method applied previously to the isotropic case,[5] Papadakis calculated curves of diffraction loss vs distance as a function of elastic anisotropy for longitudinal waves propagating along certain pure-mode axes. The deviations from exponential loss observed in pulse-echo measurements on several crystals having low intrinsic loss were adequately explained by these calculations.

This paper describes an investigation of the diffraction of 100–500-Mc/sec longitudinal elastic waves in anisotropic materials, using the techniques of optical (Bragg) scattering, which allow direct measurement of ultrasonic intensity distributions along the path of the beam.[6,7] Such measured distributions for beams propagating along pure-mode axes in crystal quartz, silicon, and potassium bromide are shown to agree very well with intensity distributions predicted using a diffraction integral similar to that used by Papadakis but derived from a rigorous solution of the related problem of electromagnetic diffraction in uniaxially anisotropic media.[8,9] In addition, it is demonstrated that cylindrical crystal surfaces, symmetric about the proper pure-mode axis, are appropriate excitation surfaces for cylindrically focused ultrasonic beams. The focusing properties of thin-film CdS and ZnO transducers evaporated on cylindrical surfaces of crystal quartz and silicon are described and compared with the properties of focused beams in isotropic materials.[7]

It has been shown[10] that simple cylindrical focusing structures can provide the enhanced ultrasonic intensities required for efficient elasto-optic light modulation. The extension of these focusing properties to anisotropic materials is of interest since many of the better modulation materials are also anisotropic.[11]

THEORY OF ULTRASONIC DIFFRACTION IN ANISOTROPIC MEDIA

The Rayleigh–Sommerfeld[8] diffraction integral allows the calculation of the electromagnetic field at a point away from an aperture in terms of the field distribution on the aperture and is an exact formulation of Huygens' principle for isotropic media. When applied to the ultrasonic case, this diffraction integra becomes

$$\bar{S}(x, y, z)\exp(-iKx) = \frac{iK}{2\pi}\iint_{\sigma} dy_0 dz_0 \bar{S}(0, y_0, z_0)\begin{pmatrix} x \\ r \end{pmatrix}\frac{\exp(-i\mathbf{K}\cdot\mathbf{r})}{r}, \quad (1)$$

relating the complex amplitude $\bar{S}(x, y, z)$ at the observation point (x, y, z) to the complex amplitude $\bar{S}(0, y_0, z_0)$ on the transducer area σ, where the distance between the source point and observation point is (Fig. 1)

$$r=[x^2+(y-y_0)^2+(z-z_0)^2]^{1/2}.$$

[1] M. J. P. Musgrave, Proc. Roy. Soc. (London) **A226,** 339, 356 (1954).
[2] H. J. McSkimin, *Physical Acoustics*, Warren P. Mason, Ed. (Academic Press Inc., New York, 1964), Vol. I, Part A.
[3] P. C. Waterman, Phys. Rev. **113,** 1240 (1959).
[4] E. P. Papadakis, J. Acoust. Soc. Am. **35,** 490 (1963); **36,** 414 (1964); **40,** 863 (1966).
[5] H. Seki, A. Granato, and R. Truell, J. Acoust. Soc. Am. **28,** 230 (1956).
[6] M. G. Cohen and E. I. Gordon, Bell Syst. Tech. J. **44,** 693 (1965).
[7] M. G. Cohen and E. I. Gordon, J. Appl. Phys. **38,** 2340 (1967).
[8] A. Sommerfeld, *Optics* (Academic Press Inc., New York, 1964).
[9] L. Bergstein and T. Zachos, J. Opt. Soc. Am. **56,** 931 (1966).
[10] E. I. Gordon, J. Quant. Electron **QE-2,** 104 (1966).
[11] R. W. Dixon and M. G. Cohen, Appl. Phys. Letters **8,** 205 (1966)

Downloaded 17 Jan 2006 to 129.49.56.176. Redistribution subject to AIP license or copyright, see http://jap.aip.org/jap/copyright.jsp

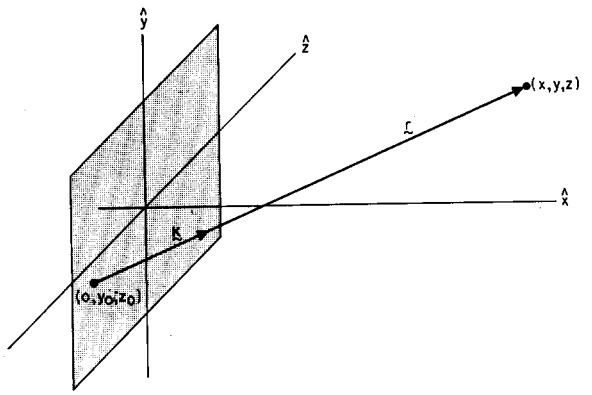

FIG. 1. Geometry of ultrasonic diffraction problem in isotropic media.

Consistent with the definitions in Ref. 6, $\bar{S}=S_c-iS_s$, where the real ultrasonic strain-wave amplitude has been written

$$S(x, y, z, t)=S_c(x, y, z)\cos(\Omega t-Kx)+S_s(x, y, z)\sin(\Omega t-Kx).$$

The ultrasonic wavevector magnitude is $K=2\pi/\Lambda=\Omega/V$ with Λ, Ω, and V defined as the ultrasonic wavelength, angular frequency and velocity, respectively. Equation (1) with $\mathbf{K}\cdot\mathbf{r}=Kr$ has been used successfully in ultrasonic diffraction studies in isotropic materials.[12,7]

While Huygens himself adapted his graphical construction to optically uniaxial media, the mathematical formulation of his principle for this case is more recent.[8,9] It is of interest here because the well-known ellipsoid of wave normals (index ellipsoid or optical indicatrix) can be shown to approximate a parabaloid for waves propagating in a direction close to the optic axis. Since this is also the approximate shape of the wave normal surface appropriate to longitudinal ultrasonic waves propagating close to three-, four-, and sixfold pure mode axes,[4] the diffraction integral derived for the optically uniaxial case is expected to apply to these elastically anisotropic cases as well. The remainder of this section will be devoted to the reformulation of the results in Ref. 9 to yield an ultrasonic diffraction integral for anisotropic media and the analytical solution of this integral for the strain intensity both in the field of a uniform plane transducer and in the focal region of a cylindrical transducer.

Using the method of angular superposition of plane waves, Bergstein and Zachos[9] obtained a Huygens' principle for the TM[13] field amplitude, or the extraordinary wave amplitude, in uniaxially anisotropic media that expressed the amplitude at an observation point, $f(x, y, z)$, in terms of the amplitude on an aperture, $f(0, y_0, z_0)$. This solution, for the special case where the optic axis is normal to an aperture in the plane $x=0$ is

$$f(x, y, z)=\frac{ik_0}{2\pi}\iint_\sigma dy_0dz_0f(0, y_0, z_0)\left(\frac{x}{r_e}\right)\frac{\exp(-ik_er_e)}{r_e}, \tag{2}$$

consistent with the coordinate notation in Fig. 1. The ordinary and extraordinary wave vectors are $k_0=2\pi n_0/\lambda$ and $k_e=2\pi n_e/\lambda$, respectively, where λ is the free space optical wavelength, and n_0 and n_e are the ordinary and extraordinary indices of refraction. Note that the form of (2) is similar to that of (1) for the isotropic case except that instead of r, the distance between source and observation points, the analysis yields,

$$r_e=[(y-y_0)^2+(z-z_0)^2+x^2(n_0^2/n_e^2)]^{1/2}.$$

The connection to the ultrasonic case is now readily made by restricting (2) to consideration of propagation directions close to the optic axis.

Consider the ellipse in Fig. 2 resulting from the projection of the optical index ellipsoid on the plane of incidence. The major and minor axes are the extraordinary and ordinary indices, n_e and n_0, respectively. The index, $n(\theta)$, appropriate to an extraordinary wave with wavevector (or wave normal) propagating at an angle θ with respect to the optic axis is

$$1/n^2(\theta)=(\cos^2\theta/n_0^2)+(\sin^2\theta/n_e^2).$$

For small θ,

$$n(\theta)\cong n_0\{1+\tfrac{1}{2}[(n_e^2-n_0^2/n_e^2]\theta^2\}.$$

The optical wavevector magnitude, $k(\theta)$, can then be

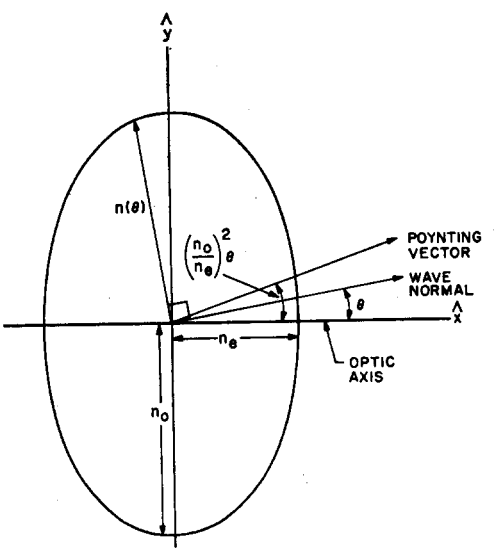

FIG. 2. Projection of index ellipsoid on plane of incidence in optically uniaxial medium.

[12] A. Freedman, J. Acoust. Soc. Am. **32**, 197 (1960); W. G. Neubauer, *ibid.* **38**, 671 (1965).

[13] For the transverse magnetic (TM) field, the component of the magnetic field vector in the direction of the optic axis is identically zero. Hence the electric field vector lies *in* the plane formed by the optic axis and the wave normal as is appropriate for an extraordinary wave.

Downloaded 17 Jan 2006 to 129.49.56.176. Redistribution subject to AIP license or copyright, see http://jap.aip.org/jap/copyright.jsp

written

$$k(\theta)=k_0\{1+\tfrac{1}{2}[(n_e^2-n_0^2)/n_e^2]\theta^2\}. \quad (3)$$

The optical energy flows in the direction of the Poynting vector (Fig. 2) which can be shown to deviate from the optic axis by the angle $(n_0/n_e)^2\theta$ when the wavevector deviates by θ.

For propagating directions close to a three-, four-, or sixfold pure-mode axis in elastically anisotropic media, the longitudinal ultrasonic wavevector magnitude, $K(\theta)$ is

$$K(\theta)=K_0(1+b\theta^2), \quad (4)$$

derived by Papadakis[4] for small values of θ, the angle between the wave vector direction and the pure-mode axis. This follows immediately from Waterman's[3] solution for the ultrasonic phase velocity

$$V(\theta)=V_0(1-b\theta^2),$$

where V_0 and $K_0=\Omega/V_0=2\pi/\Lambda_0$ are the pure-mode velocity and wavevector magnitude, respectively, and Λ_0 is the pure-mode wavelength. The anisotropy parameter b is a function of the elastic moduli and is tabulated in Ref. 4 for the pure-mode axis and crystal symmetry of interest. The ultrasonic energy flows in the direction of the elastic Poynting vector $\mathbf{P}$ which deviates from $\mathbf{K}$ by the angle d_p.[4] When $\mathbf{K}$ deviates from the pure mode axis by the angle θ, $d_p=-2b\theta$, so that $\mathbf{P}$ deviates from the pure-mode axis by $(1-2b)\theta$.

Comparison of (3) and (4) establishes the equivalent angular dependences of the optical and ultrasonic wave vector magnitudes. The substitution

$$\tfrac{1}{2}(n_e^2-n_0^2)/n_e^2\rightarrow b \quad (5)$$

indicated as necessary by this equivalence to modify (2) to the ultrasonic case, is also consistent with the equivalent dependence of the optical and ultrasonic Poynting vector directions on their respective wavevector directions.

If, in addition to (5),

$$k_0\rightarrow K_0 \quad \text{and} \quad k_e=(n_e/n_0)k_0\rightarrow K_0/(1-2b)^{1/2},$$

then the diffraction integral (2) rewritten for elastically

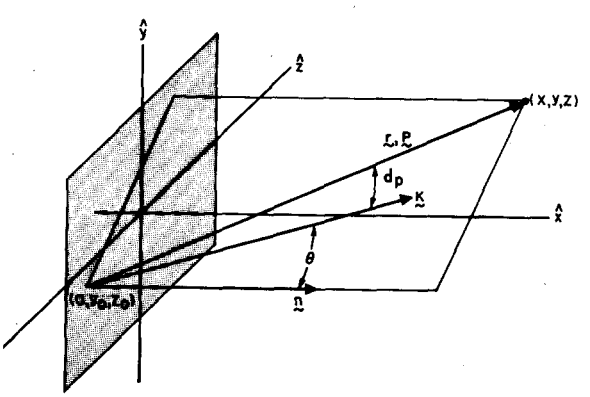

FIG. 3. Geometry of ultrasonic diffraction problem in anisotropic media.

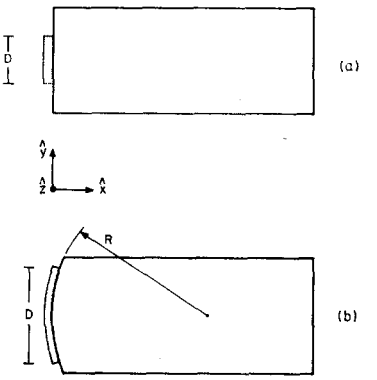

FIG. 4. (a) Diffraction structure with plane transducer. (b) Focusing structure with cylindrical transducer.

anisotropic media becomes, for small θ,

$$\bar{S}(x,y,z)\exp(-iK_0x)=\frac{iK_0}{2\pi}\iint_\sigma dy_0dz_0\bar{S}(0,y_0,z_0)\left(\frac{x}{r_e}\right)\times\frac{\exp[-iK_0r_e/(1-2b)^{1/2}]}{r_e}, \quad (6)$$

where now $r_e=[(y-y_0)^2+(z-z_0)^2+x^2(1-2b)]^{1/2}$. The pure-mode axis is normal to the transducer area σ. Since the Fresnel region is of interest experimentally and (6) is valid there, it is appropriate to write

$$r_e\cong x(1-2b)^{1/2}+\frac{(y-y_0)^2}{2x(1-2b)^{1/2}}+\frac{(z-z_0)^2}{2x(1-2b)^{1/2}}$$

in the exponential, and $r_e=x(1-2b)^{1/2}$ elsewhere in (6). The resulting integral

$$\bar{S}(x,y,z)=\frac{iK_0}{2\pi x(1-2b)}\iint_\sigma dy_0dz_0\bar{S}(0,y_0,z_0)\times\exp\left(-iK_0\left[\frac{(y-y_0)^2}{2x(1-2b)}+\frac{(z-z_0)^2}{2x(1-2b)}\right]\right) \quad (7)$$

is readily evaluated for a uniform plane transducer and for a cylindrical focusing transducer.

Before proceeding with this evaluation, it should be mentioned that Papadakis obtained a similar integral simply by introducing the anisotropy into the exponent in (1). Using (4) and the fact that the Poynting vector $\mathbf{P}$ (and hence $\mathbf{r}$), $\mathbf{K}$, and $\mathbf{n}$, the transducer normal, are coplanar (Fig. 3), the dot product $\mathbf{K}\cdot\mathbf{r}$ becomes, for small θ

$$\mathbf{K}\cdot\mathbf{r}=K_0r[1+b(1-2b)\theta^2], \quad (8)$$

using $d_p=-2b\theta$. Substituting (8) into (1) can be shown to yield the diffraction formula (7) in the Fresnel region except for the constant factor $(1-2b)^{-1}$ multiplying the integral. Papadakis established the validity of this approach by comparing calculated results with experimental data. The discussion above establishes (7) as a rigorously correct diffraction formula.

For the plane transducer [Fig. 4(a)]

$$\bar{S}(0,y_0,z_0)=\bar{S}_0 \quad -\tfrac{1}{2}D\leq y_0\leq\tfrac{1}{2}D$$
$$=0 \quad \text{elsewhere}, \quad (9)$$

Downloaded 17 Jan 2006 to 129.49.56.176. Redistribution subject to AIP license or copyright, see http://jap.aip.org/jap/copyright.jsp

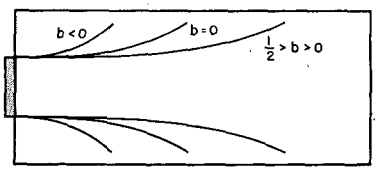

FIG. 5. Schematic illustration of diffraction of ultrasonic beams generated by a plane transducer in media with $b<0$, $b=0$, and $\frac{1}{2}>b>0$.

and $\bar{S}_0$ is a constant. For the focusing transducer, [Fig. 4(b)] taking the axis of the cylindrical surface with radius of curvature R parallel to $\hat{z}$

$$\bar{S}(0, y_0, z_0) = \bar{S}_0 \exp(iK_0 y_0^2/2R) \qquad -\tfrac{1}{2}D \leq y_0 \leq \tfrac{1}{2}D$$
$$= 0 \qquad \text{elsewhere,} \qquad (10)$$

and again $\bar{S}_0$ is constant. The integral over z_0 in (7) may be immediately performed from $-\infty$ to $+\infty$ with no loss of generality.[14] Then, using (9), the ultrasonic intensity in the field of a plane transducer is

$$|\bar{S}(x, y)|^2 = |\bar{S}_0|^2 \left| \sqrt{2}^{-1} \int_{v_-}^{v_+} dv \exp -\tfrac{1}{2}(i\pi v^2) \right|^2, \qquad (11)$$

where

$$v = \left[\frac{2}{\Lambda_0 x(1-2b)}\right]^{1/2} (y_0 - y)$$

$$\text{and } v_\pm = \left(\frac{2}{\Lambda_0 x(1-2b)}\right)^{1/2} (\pm\tfrac{1}{2}D - y). \qquad (12)$$

The integral in (11) is just the combination of Fresnel integrals that results in the analogous calculation of the near-field amplitude distribution of a uniformly illuminated slit. The predicted intensity distribution at a distance x from the source is equivalent to the distribution predicted in the optical[15] or elastically isotropic[12] case at a distance $x(1-2b)$. For negative values of b, $1-2b$ is greater than unity, indicating that the far-field intensity distribution is closer to the transducer than it is in the isotropic case, $b=0$ (Fig. 5). This is consistent with the deviation of the Poynting vector away from **K** and the pure-mode axis for negative b. Similarly, in media with positive b, the ultrasonic beam spreads out less rapidly than in the isotropic case. Values of b that have been computed[4] range from $b=-5.23$ for propagation along the c axis in Zn to $b=+0.38$ for ⟨100⟩ propagation in KI, indicating that the diffraction spreads in Fig. 5 represent real situations and have not been exaggerated for clarity. Unfortunately, b appears restricted to values less than $\frac{1}{2}$,[4] so that it is not possible to find a completely self-collimating medium.

For the focusing case, (7) is readily evaluated in the plane $x=R/(1-2b)$ and gives, for the focal plane intensity,

$$\left|\bar{S}\left(\frac{R}{1-2b}, y\right)\right|^2 = |\bar{S}_0|^2 \frac{D^2}{R\Lambda_0} \frac{\sin^2 \tfrac{1}{2}K_0 Dy/R}{(\tfrac{1}{2}K_0 Dy/R)^2}. \qquad (13)$$

The energy focuses cleanly to a $(\sin X/X)^2$ distribution on the axis at the intersection of the Poynting vectors (Fig. 6). The focal distance is less than or greater than R depending on the sign of b but the distribution's peak-to-zero width, $w=R\Lambda_0/D$, and peak intensity, $|\bar{S}_0|^2 D^2/R\Lambda_0$, are equal to the values expected for $b=0$, the isotropic case.

EXPERIMENTAL RESULTS

Experiments in crystals with both positive and negative values of b were performed to confirm (11) for the plane transducer and (13) for the focusing transducer. For negative b, longitudinal waves were propagated along the three fold axis in crystal quartz. If Bechmann's[16] measured values of the elastic moduli are used with

$$b = (c_{33}-c_{13}-2c_{44})(c_{33}+c_{13})/2c_{33}(c_{33}-c_{44}),$$

then $b=-0.232$. The threefold ⟨111⟩ axis in silicon provided one case of positive b,

$$b = \frac{2(2c_{44}+c_{12}-c_{11})(c_{11}+2c_{12}+c_{44})}{3(c_{12}+c_{44})(c_{11}+2c_{12}+4c_{44})} = 0.162$$

using Ref. 17; and the fourfold ⟨100⟩ axis of KBr provided

$$b = \frac{(c_{11}-c_{12}-2c_{44})(c_{11}+c_{12})}{2c_{11}(c_{11}-c_{44})} = 0.373$$

substituting the c_{ij} values of Galt.[18]

The experimental arrangement, shown in Fig. 7, has been described in detail previously.[11,7] As mentioned above, the laser beam, cylindrically focused to less than 0.02 mm in height, and incident approximately along

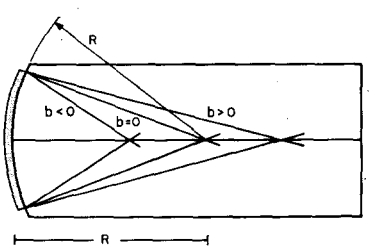

FIG. 6. Schematic illustration of focusing of ultrasonic beams in media with $b<0$, $b=0$, and $\frac{1}{2}>b>0$.

[14] The results of experiments performed to determine the intensity profiles of the thin-film transducers used here agreed with previous findings[7] that $\bar{S}_0(0, y_0, z_0)$ can be assuned relatively constant and independent of z. Since the probing light beam is incident essentially normal to the plane of Fig. 4 and is translated across the ultrasonic beam in the $\hat{y}$ direction, an integration of the intensity along $\hat{z}$ results. Hence, the measured intensity distributions are a function of y and x only.

[15] F. Jenkins and H. White, *Fundamentals of Optics* (McGraw-Hill Book Company, Inc., New York, 1957), 3rd. ed..

[16] R. Bechmann, Phys. Rev. **110**, 1060 (1958).

[17] H. J. McSkimin, J. Appl. Phys. **24**, 988 (1953).

[18] J. K. Galt, Phys. Rev. **73**, 1460 (1948).

Downloaded 17 Jan 2006 to 129.49.56.176. Redistribution subject to AIP license or copyright, see http://jap.aip.org/jap/copyright.jsp

$\hat{z}$, was translated across the ultrasonic beam in the $\hat{y}$ direction. The ultrasonic intensity distributions at various positions along the beam were determined by measuring the Bragg-scattered light intensity distributions. The He–Ne laser beams, 6238 Å for the quartz and KBr and 1.15 μ for the Si,[19] were apertured to $\frac{1}{2}$mm in the $\hat{x}$ direction so that the value of x could be accurately selected. Evaporated thin-film CdS transducers were applied to the quartz structures while sputtered ZnO films were available for use with the Si samples. An X-cut 20-Mc fundamental, quartz transducer, bonded with phenyl salicylate (salol) to a ⟨100⟩ face, was a satisfactory plane transducer for the KBr crystal. No focusing was attempted in this material. In each case, an evaporated gold-back electrode determined the active transducer height D.

Typical experimental data for the plane transducers are presented in terms of the parameter $\Delta v = v_+ - v_-$ and are summarized in Table I. The values of Δv_{calc} were computed using (12) and are seen to compare quite favorably with the Δv_{exp} values assigned to the traces. This latter assignment was performed by matching the experimental curves [see Figs. 8(a), (b) for quartz and 9(a), (b) for Si] with computer-drawn curves of

$$\frac{1}{2}\left|\int_{\Delta v}\exp(-\tfrac{1}{2}i\pi v^2)\,dv\right|^2$$

[see Figs. 8(c) and 9(c)]. The KBr distribution (Fig. 10) was matched with Fig. 18U in Ref. 14. Since details of these diffraction patterns are sensitive to the intensity profile of the transducer, the asymmetries seen are attributed to the small nonuniformities measured over the transducer area. This lack of complete uniformity was noticeable mainly with the

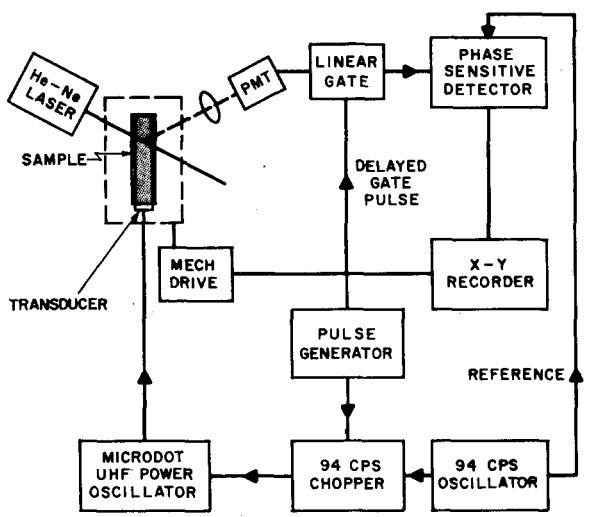

FIG. 7. Experimental arrangement for measurement of ultrasonic intensity distributions using Bragg scattering.

[19] Intrinsic optical loss for 5-mm path lengths in the high resistivity ($\rho > 1000\,\Omega\cdot$cm) samples used was ~10%.

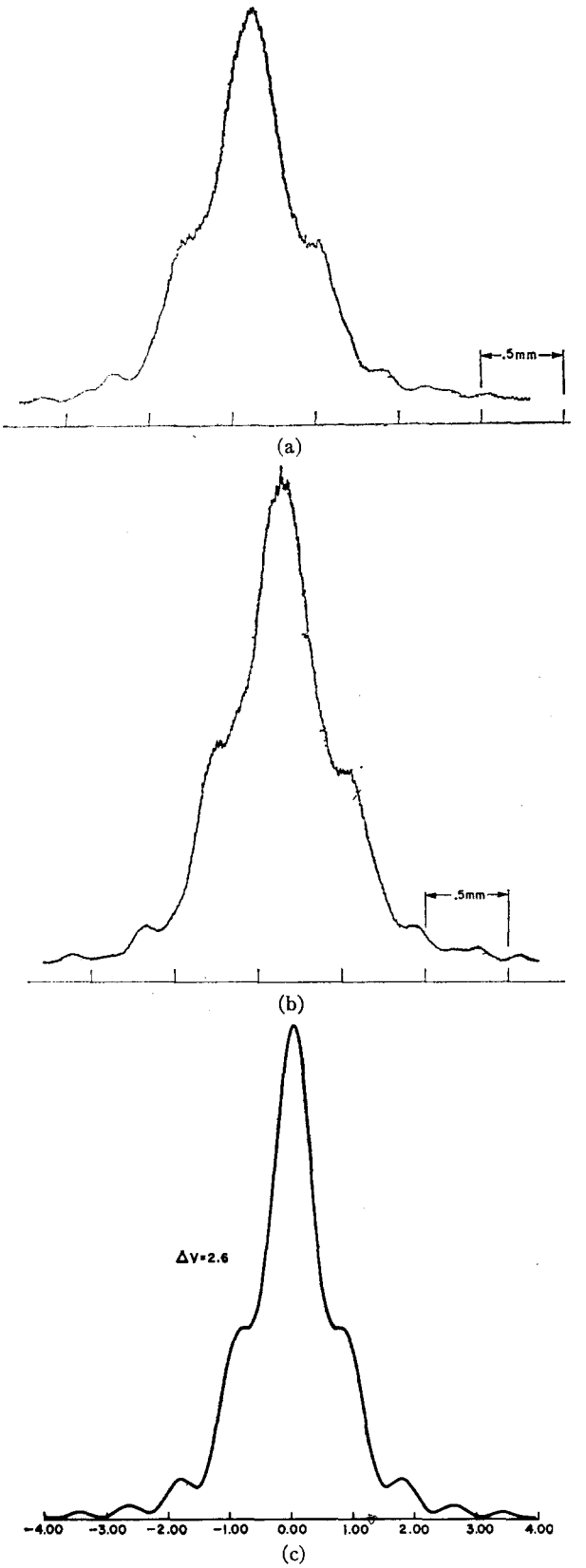

FIG. 8. Ultrasonic intensity distribution of plane transducer (a) Measured in crystal quartz at 150 Mc/sec (see Table I). (b) Measured in crystal quartz at 300 Mc/sec (see Table I). (c) Computed from Eq. (11) for $\Delta v = 2.60$ with $|S_0|^2 = 1$.

Downloaded 17 Jan 2006 to 129.49.56.176. Redistribution subject to AIP license or copyright, see http://jap.aip.org/jap/copyright.jsp

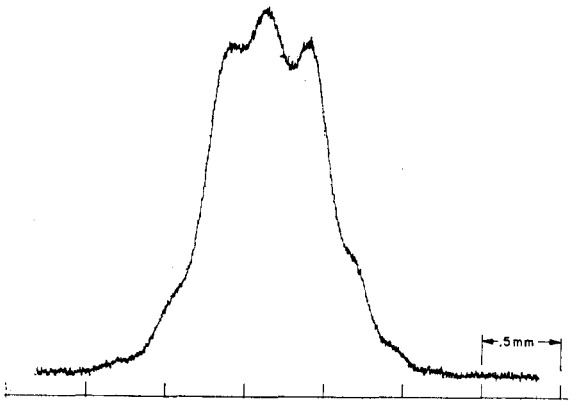

(a)

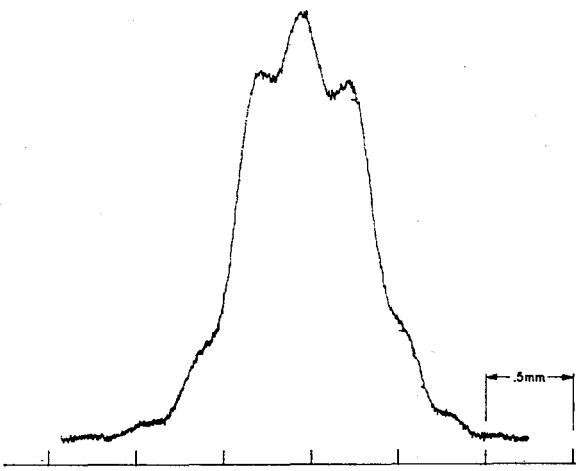

(b)

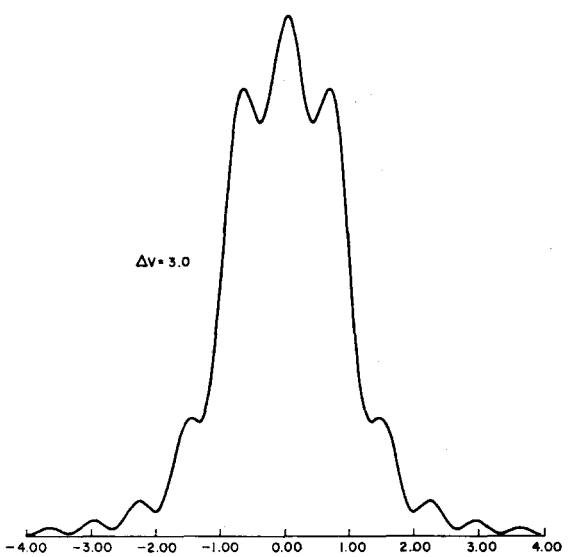

(c)

FIG. 9. Ultrasonic intensity distribution of plane transducer (a) Measured in silicon at 150 Mc/sec (see Table I). (b) Measured in silicon at 250 Mc/sec (see Table I). (c) Computed from Eq. (11) for $\Delta v=3.0$ with $|\tilde{S}_0|^2=1$.

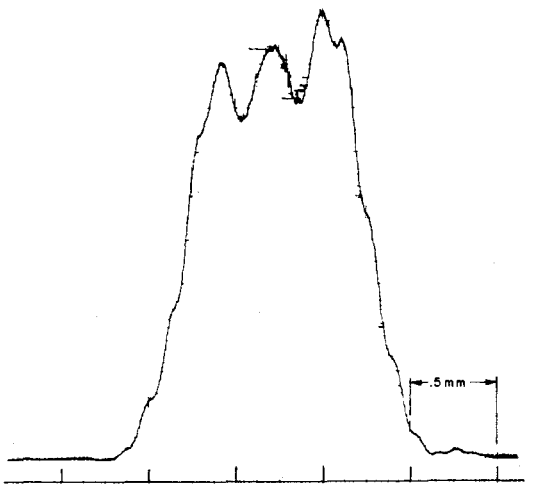

FIG. 10. Ultrasonic intensity distribution of plane transducer in KBr at 100 Mc/sec (see Table I).

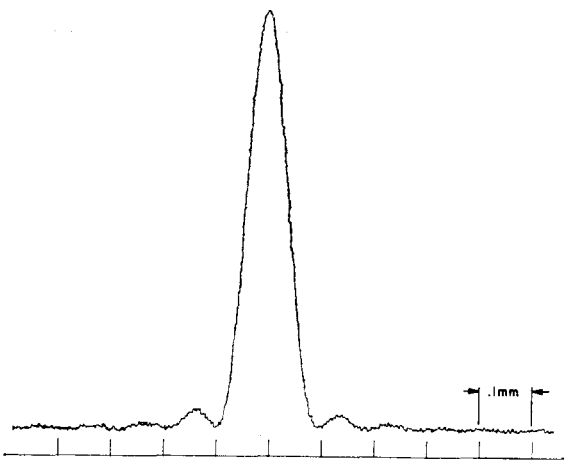

FIG. 11. Ultrasonic intensity distribution in focal plane of cylindrical transducer in crystal quartz at 500 Mc/sec (see Table II).

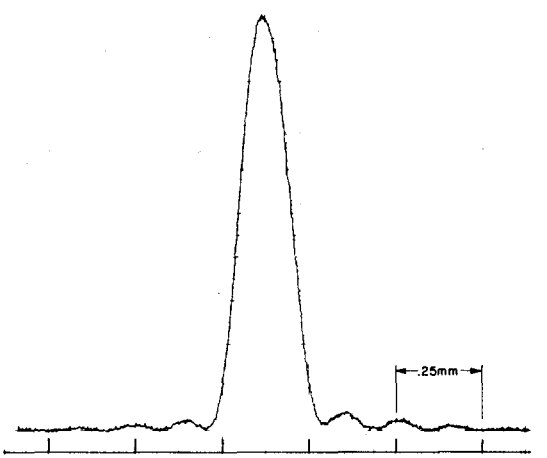

FIG. 12. Ultrasonic intensity distribution in focal plane of cylindrical transducer in silicon at 300 Mc/sec (see Table II).

Downloaded 17 Jan 2006 to 129.49.56.176. Redistribution subject to AIP license or copyright, see http://jap.aip.org/jap/copyright.jsp

TABLE I. Plane transducer.

Sample	f (Mc/sec)	D (cm)	x (cm)	Δv_{calc}	Δv_{exp}
Quartz (z axis)	150	0.114	0.635	2.56	2.60
Quartz (z axis)	300	0.114	1.270	2.56	2.60
Si ⟨111⟩	150	0.120	0.740	3.05	3.00
Si ⟨111⟩	250	0.120	1.245	3.02	3.00
KBr ⟨100⟩	100	0.116	1.523	4.40	4.60

KBr sample where difficulty was encountered with the salol bond.

Intensity distributions in the focal plane of the cylindrical transducers in quartz and Si are shown in Figs. 11 and 12, respectively. Table II summarizes some of the relevant data and indicates good quantitative agreement between theory and experiment. The energy focused at χ_f, close to the predicted value $R/(1-2b)$, and had a $(\sin X/X)^2$ distribution with width w appropriate to the isotropic case, $b=0$. Again the lack of complete symmetry and other small deviations from perfect $(\sin X/X)^2$ behavior have been attributed to slight nonuniformities in the transducer intensity profiles.

The technique of Bragg scattering has demonstrated its effectiveness in probing angular as well as linear ultrasonic intensity distributions. By varying the angle between the ultrasonic beam and a (wide) probing light beam about the Bragg angle and monitoring the scattered light intensity, the angular distribution of ultrasonic $\mathbf{K}$ vectors is measured.[6] In isotropic materials, this distribution is equivalent to the angular distribution of Poynting vectors or the intensity distribution in the far field of the ultrasonic beam. As indicated above, in anisotropic materials near certain pure-mode axes, these distributions are no longer equivalent but are simply related via the anisotropy parameter b. Since the Poynting vector (Fig. 3) deviates by $\theta+d_p=(1-2b)\theta$ from the pure-mode axis when the wave vector $\mathbf{K}$ deviates by θ, the angular distribution of $\mathbf{K}$ vectors for an aperture should be equal to $1/(1-2b)$ of the angular width of the far-field intensity distribution of the aperture. In particular, for a transducer of height D, solution of (7) in the far-field limit, neglecting terms in y^2 and y_0^2, yields

$$|\bar{S}(x,y)|^2=|\bar{S}_0|^2\frac{D^2}{x(1-2b)\Lambda_0}\frac{\sin^2\frac{1}{2}K_0Dy/x(1-2b)}{(\frac{1}{2}K_0Dy/x(1-2b))^2} \tag{14}$$

for the far-field intensity distribution. The results of an experiment performed in quartz by rotating the crystal about the Bragg angle with the light beam in the plane of Fig. 4(a) indicate, as expected, that the $\mathbf{K}$ vector angular distribution has a peak-to-first zero angular width Λ_0/D compared to the angular width of the far-field intensity distribution, $(1-2b)\Lambda_0/D$, calculated from (14) and verified experimentally.

The analysis in Sec. II was performed for the special case of perfect alignment of the pure-mode axis along $\hat{x}$. In a real experimental situation some misalignment is inevitable. To the degree of approximation considered above, an angular deviation, ϕ, between $\hat{x}$ and the pure-mode axis results only in an angular deviation of the ultrasonic beam (unfocused or focused) of $(1-2b)\phi$ from $\hat{x}$. Otherwise, diffraction and focusing of the beam are unchanged. The parabolic approximation (4) appears to apply reasonably well to values of θ of at least 6°; hence misorientation of 1° or 2° should not produce noticeable effects. While the quartz samples used above were oriented to better than 1 min of arc, the ⟨111⟩ axis of one of the Si crystals deviated from the transducer face by 1.2° as measured with an x-ray goniometer. The diffraction properties of this latter sample were not observably modified.

TABLE II. Focusing transducer.

Sample	f (Mc/sec)	D (cm)	R (cm)	$R/(1-2b)$ (cm)	x_f (cm)	w_{calc} (mm)	w_{exp} (mm)
Quartz (z axis)	500	0.250	1.810	1.252	1.240	0.094	0.098
Si ⟨111⟩	300	0.404	1.975	2.920	3.020	0.153	0.166
Si ⟨111⟩	350	0.406	2.021	2.990	2.900	0.133	0.144

Downloaded 17 Jan 2006 to 129.49.56.176. Redistribution subject to AIP license or copyright, see http://jap.aip.org/jap/copyright.jsp

CONCLUSION

A diffraction integral for longitudinal ultrasonic waves propagating along three-, four-, or sixfold pure-mode axes in single crystals has been derived using a solution available from optical diffraction theory for uniaxially anisotropic media. Intensity distributions in the field of a uniform plane transducer predicted using this diffraction integral agreed very well with the measured distributions in quartz, silicon, and KBr. In addition, the focusing properties of cylindrical transducers, symmetric about proper pure-mode axes in quartz and silicon were described and compared with the properties of isotropic focusers.

ACKNOWLEDGMENTS

The samples used were expertly fabricated by T. Kunz and the CdS and ZnO films were evaporated by J. Wagner and N. F. Foster. An informative discussion with T. Zachos and the critical readings of the manuscript by E. I. Gordon and R. W. Dixon are also gratefully acknowledged.

JOURNAL OF APPLIED PHYSICS VOLUME 38, NUMBER 10 SEPTEMBER 1967

Initial Shock-Front Interaction with Solid Models

WALTER ZAGIEBOYLO

Pioneering Research Division, U. S. Army Natick Laboratories, Natick, Massachusetts

(Received 19 September 1967; in final form 1 May 1967)

The initial response of solid models to low-Mach, high-mass-flow shock waves was analyzed. A rapid-response piezoelectric load cell was mounted in a series assembly behind the models to directly measure resultant loading. The load history was analyzed and correlated with model geometry and shock-wave velocity for rectangular wood models of various length and weight and for the effects caused by changing the front surface material. The front surface of the model was in some cases bare and in other cases covered with plastic foam or thin foam rubber. It was observed that the coatings produced increased loading effects. The maximum loading force was determined for various overpressures and found to be in linear relationship to a dimensionless ratio involving shock-tube and shock-wave pressure parameters.

INTRODUCTION

The blast-effect parameters of nuclear bursts have been intensively studied over the past decade. Much of the theoretical analysis of nuclear shock waves was an extension of shock-tube studies and shock tubes have been used in attempts to simulate the shock waves generated by nuclear explosions. Because the nuclear shock wave is of much longer duration than most shock-tube waves, scaling of model effects is generally difficult; however, the initial response of a model in a shock tube can be identical to the response of the model to a nuclear shock in the region of Mach reflection.[1] The blast loading on models is a function of peak overpressure, dynamic pressure, decay, and duration as well as size, shape, orientation, and response of the model. Theoretical interaction of the incident blast with idealized models has been developed primarily from data obtained in shock tubes and wind tunnels, and air-blast loading on idealized models of simple shape have been calculated.[2]

This report deals with the direct measurement of the impulsive loading response of simple models to shock waves in air. It is limited to the loading that takes place during the initial diffraction process before the shock front passes the model rear surface. Initially the exposed model is subjected to the high reflected pressure on its front surface. The limited diffraction process ends as the shock wave begins loading the model back surface. After this phase, the net loading on the model restraints is determined by the model shape and the dynamic pressure and blast wave duration. As models become smaller, or the positive phase of the blast wave becomes longer (nuclear weapons of larger yield), drag loading is the important destruction criterion. These effects are difficult to measure and to scale in shock-tube model work. Diffraction targets, such as those targets exposed to relatively short-duration nuclear weapons, can be more accurately scaled, and the effect of this loading has been directly measured for simple models.

PROCEDURE

The U.S. Army Natick Laboratories shock tube[3] was used to generate low-Mach shock waves in a 4×15-in. cross section. A typical model is shown in Fig. 1. The model assembly is positioned about 6½ ft

[1] S. Glasstone, *The Effects of Nuclear Weapons* (Department of Defense and U. S. Atomic Energy Commission, U. S. Government Printing Office, 1962).

[2] W. Bleakney, D. R. White, and W. C. Griffith, J. Appl. Mech. **17**, 439 (1950).

[3] W. Zagieboylo and S. D. Tanenholtz, U. S. Army Natick Laboratories, Report S-1, February 1964.

Downloaded 17 Jan 2006 to 129.49.56.176. Redistribution subject to AIP license or copyright, see http://jap.aip.org/jap/copyright.jsp